Surface Roughness Effects on Equilibrium Temperature of Interacting Surfaces

R. G. HERING* AND T. F. SMITH†
University of Illinois at Urbana-Champaign, Urbana, Ill.

A simple system of radiatively interacting, one-dimensionally rough surfaces in the presence of a collimated solar flux is considered. Rough surface properties depend on material solar absorptance (α_w), roughness element slope, and roughness element specularity. Numerical solution to the governing integral equation for solar radiant intensity leads to equilibrium temperature distributions for a range of each influencing roughness parameter. The equilibrium temperature results demonstrate that roughness effects are, relatively unimportant for high-α_w materials, while, for low-α_w materials, surface roughness can change local temperature by 50%. When surface roughness effects on radiative properties are completely ignored in engineering analysis, acceptable accuracy is achieved only for high-α_w materials. An approximate method of analysis employing rough surface apparent directional absorptance for directly incident solar energy generally gave acceptable engineering accuracy throughout the entire range of α_w. Neither method of analysis, however, yields an acceptable approimation to rough surface temperature for low-α_w materials when a large fraction of directly incident solar energy is back-scattered to the environment.

Nomenclature

dA = plate surface area element
G = absorbed solar irradiation
$\mathcal{G}$ = dimensionless absorbed solar energy, G/S
H = intensity ratio $I^+/(S/\pi)$
I^+,I^- = intensities of emergent and incident solar energies
l = plate length
S = solar constant
T = local equilibrium temperature
x,y = coordinates
α = solar absorptance
β = dimensionless solar radiosity
γ = included angle
ϵ = infrared emittance
Θ = dimensionless equilibrium temperature $T/(S/\sigma)^{1/4}$
θ,θ' = angles of emergent and incident energies
$\theta_{\lim}'$ = limiting angle of incident solar energy
θ_s' = direction of directly incident solar energy
ξ,η = dimensionless coordinates x/l and y/l
ρ = solar reflectance
ρ_{bd} = bidirectional reflectance
σ = Stefan-Boltzmann radiation constant
χ = roughness element included angle
$d\omega,d\omega'$ = solid angle increments of emergent and incident solar energies

Subscript

a,w = apparent and wall, respectively

Superscript

D,S = diffuse and specular components, respectively

Introduction

SURFACE topography contributes to the difference between thermal radiation properties of engineering materials and property models commonly employed in analysis of radiative transfer between opaque surfaces. Roughness influences both the amount of energy emitted and reflected relative to that of the constituent material, as well as the spatial distribution of these energies. Since methods employed to evaluate equilibrium temperature generally do not account for such effects, these techniques may lead to significant differences between predicted and observed equilibrium temperatures. Recently, all apparent thermal radiation properties required to implement studies of surface roughness effects on radiative transfer were reported for a one-dimensionally rough surface.[1] These properties have been used to evaluate surface roughness effects on radiative heat transfer and equilibrium temperature of isolated surfaces,[2,3] as well as radiative heat transfer between interacting surfaces[4,5] in the absence of external radiation fields. This study utilizes the apparent properties to assess the influence and importance of surface roughness on the equilibrium temperature distribution acquired in a system of interacting surfaces in the presence of a collimated solar flux and to evaluate the magnitude of the discrepancy in temperature incurred when simple property models are used.

The system selected for study (Fig. 1) consists of identical equal-length plates of infinite width sharing a common edge. A uniform collimated solar flux is directed along the bisector of the included angle γ. Both surfaces

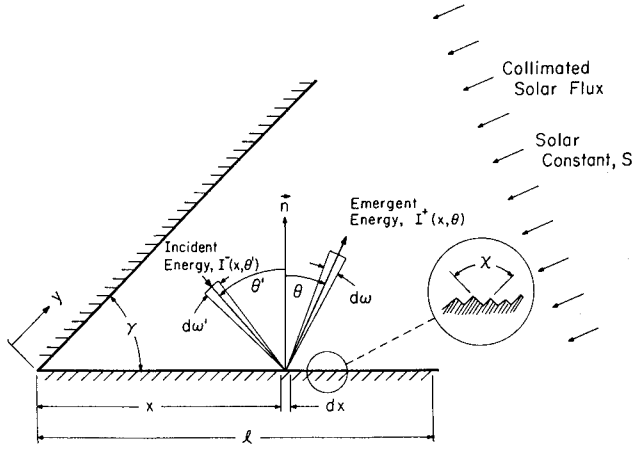

Fig. 1 Schematic diagram of adjoint plate system.

Presented as paper at the AIAA 5th Thermophysics Conference, Los Angeles, Calif., June 29–July 1, 1970; submitted August 4, 1970; revision received September 25, 1970. This paper presents results of research supported in part by Jet Propulsion Laboratory, California Institute of Technology, Contract 951661.

* Professor, Department of Mechanical Engineering. Member AIAA.

† Research Assistant, Department of Mechanical Engineering.

are opaque and have identical uniform radiative properties that are temperature independent. Surface heat exchange occurs only by radiant transport through transparent media of unit refractive index. This configuration is of particular interest because of the application of results to wedge cavities, louver systems, and successive elements in an array of high-conductivity longitudinal fins. Furthermore, extensive results are available for equilibrium temperature distribution,[6] based on simple direction independent property models commonly employed in engineering radiant heat-transfer analysis. For the rough-surface radiant heat-transfer analysis reported herein, surface roughness elements are in the shape of V-grooves with axes parallel to the plate edge. Wavelengths of the incident solar flux are considered small in comparison to the characteristic length of surface roughness elements. Apparent thermal radiation properties[1] are applicable to energy transfer in the solar spectral interval. For wavelengths characteristic of the surface emission, surfaces are optically smooth, and a specular reflection model is employed to describe reflection of emitted energy. A semigray spectral property model is employed to approximate the difference in surface properties of engineering materials for solar and surface radiation.[6]

Analysis

Radiant Transfer Formulation

Consider area element $dA(= dx\ dz)$ located distance x from the common edge of the plates. The temperature acquired by this element under adiabatic conditions is determined by equality of emitted energy to rate of absorption of incident energy. For the system selected for study, local temperature is governed by the following integral equation[6]:

$$\epsilon\sigma T^4(x) = G(x) + \epsilon^2 \int_0^l \sigma T^4(y) K_\gamma(x,y)dy \qquad (1)$$

The exchange factor for surface emission $K_\gamma(x,y)$ is available for included angles $\gamma = \pi/n$ with n a positive integer as[6]

$$K_\gamma(x,y) = \sum_{j=1}^{M} (1 - \epsilon)^{j-1} f_{j\gamma}(x,y) \qquad (2)$$

in which

$$f_{j\gamma}(x,y) = (xy \sin^2 j\gamma)/2(x^2 + y^2 - 2xy \cos j\gamma)^{3/2} \qquad (3)$$

and $M = n - 1$. In Eq. (1), $\epsilon\sigma T^4(x)$ represents the emissive power of the surface element, and $G(x)$ is the locally absorbed solar irradiation which, within the framework of the semigray assumption, is determined from independent analysis presented later. The remaining integral term represents absorption of energy emitted by both surfaces, which is transported to the considered surface element both directly and by all possible specular reflection paths. To evaluate $T(x)$ from Eq. (1), it is necessary to provide $G(x)$, and attention is directed to this analysis next.

Unlike analysis for diffusely or specularly reflecting surfaces, evaluation of locally absorbed solar energy for interacting rough surfaces generally requires evaluation of the spatial distribution of local radiant solar intensity. For this purpose, let θ' and θ denote arbitrary directions of incident and emergent radiant energy, respectively, measured from the mean surface normal in a plane perpendicular to the plate edge. Let $I^+(x,\theta)$ represent the intensity of radiant energy in the solar spectral interval emerging from the considered plate element per unit time and per unit area, which is confined to the solid angle increment $d\omega$ defined by the cylindrical sector subtending angular increment $d\theta$. If $I^-(x,\theta')$ denotes the analogous intensity for incident energy confined to solid angle increment $d\omega'$, emergent solar intensity is governed by the following equation[4]:

$$I^+(x,\theta) = \rho_{bd}(\theta_s',\theta) S \sin\frac{\gamma}{2} + \frac{\pi}{2} \int_{\theta_{\lim}'(x)}^{\pi/2} \rho_{bd}(\theta',\theta) I^-(x,\theta') \cos\theta' d\theta' \qquad (4)$$

where $\rho_{bd}(\theta',\theta)$ is rough surface bidirectional reflectance. In Eq. (4), $\theta_s'[= (\pi - \gamma)/2]$ is the direction of directly incident solar energy, and S denotes the solar constant. Physically, Eq. (4) states that emergent intensity at x in direction θ is the sum of directly incident solar energy which is reflected by the surface into solid angle increment $d\omega$ about direction θ and interreflected solar energy leaving the adjacent plate, which after reflection from the considered element emerges within $d\omega$. For the adjoint plate system, contributing directions for solar energy emerging from the adjacent plate are limited to a value $\theta_{\lim}'(x)$ given by,

$$\theta_{\lim}'(x) = -\tan^{-1}[\{\cos\gamma - (x/l)\}/\sin\gamma] \qquad (5)$$

Also, since the intervening medium is radiatively transparent, intensity of incident energy $I^-(x,\theta')$ is identical to intensity of emergent energy of the adjacent plate evaluated at a suitable location and direction $I^+(y,\phi)$. From geometry, it follows that

$$y/x = \cos\theta'/\cos(\theta' - \gamma) \text{ and } \phi = \theta' - \gamma \qquad (6)$$

Hence, Eq. (4) may be written

$$I^+(x,\theta) = \rho_{bd}(\theta_s',\theta) S \sin\frac{\gamma}{2} + \frac{\pi}{2} \int_{\theta_{\lim}'(x)}^{\pi/2} \rho_{bd}(\theta',\theta) \times I^+[y(x,\theta'),\phi(\theta')] \cos\theta' d\theta' \qquad (7)$$

As a result of symmetry in the system, the intensity to the left and that within the integral operator refer to the same physical quantity. Thus, Eq. (7) constitutes a linear integral equation for the angular dependence of local radiant intensity.

Once local solar intensity is available for all directions at each position on the plates, locally absorbed solar irradiation follows as

$$G(x) = \alpha_a(\theta_s') S \sin\frac{\gamma}{2} + \frac{\pi}{2} \int_{\theta_{\lim}'(x)}^{\pi/2} \alpha_a(\theta') \times I^+[y(x,\theta'),\phi(\theta')] \cos\theta' d\theta' \qquad (8)$$

In Eq. (8), $\alpha_a(\theta')$ is the directional absorptance for energy incident at polar angle θ'.

It is convenient to nondimensionalize the governing equations by introducing the following dimensionless variables:

$$\Theta(\xi) = T(x)/(S/\sigma)^{1/4},\ H(\xi,\theta) = I^+(x,\theta)/(S/\pi)$$
$$\mathcal{G}(\xi) = G(x)/S,\ \xi = x/l,\ \eta = y/l \qquad (9)$$

Using these variables in Eq. (1) yields

$$\Theta^4(\xi) = \frac{1}{\epsilon} \mathcal{G}(\xi) + \epsilon \int_0^1 \Theta^4(\eta) K_\gamma(\xi,\eta) d\eta \qquad (10)$$

with K_γ and $f_{j\gamma}$ of Eqs. (2) and (3) given by identical expressions, except for replacement of x and y with ξ and η, respectively. Dimensionless locally absorbed solar energy follows from Eq. (8) as

$$\mathcal{G}(\xi) = \alpha_a(\theta_s') \sin\frac{\gamma}{2} + \frac{1}{2} \int_{\theta_{\lim}'(\xi)}^{\pi/2} \alpha_a(\theta') \times H[\eta(\xi,\theta'),\phi(\theta')] \cos\theta' d\theta' \qquad (11)$$

with dimensionless solar intensity evaluated from

$$H(\xi,\theta) = \pi\rho_{bd}(\theta_s',\theta) \sin\frac{\gamma}{2} + \frac{\pi}{2} \int_{\theta_{\lim}'(\xi)}^{\pi/2} \rho_{bd}(\theta',\theta) \times H[\eta(\xi,\theta'),\phi(\theta')] \cos\theta' d\theta' \qquad (12)$$

Table 1 Apparent directional absorptance of rough surface for directly incident solar energy $\alpha_a(\theta_S')$

	$\theta_S' = 45°$				$\theta_S' = 67.5$			
	$\chi = 45°$		$\chi = 90°$		$\chi = 45°$		$\chi = 90°$	
α_w	$\rho_w{}^S/\rho_w = 0$	1	0	1	0	1	0	1
0.1	0.200	0.19	0.138	0.1	0.176	0.1	0.126	0.1
0.5	0.677	0.75	0.588	0.5	0.638	0.5	0.563	0.5
0.9	0.948	0.99	0.927	0.9	0.938	0.9	0.920	0.9

Approximate Formulation

In anticipation of later comparison, it is of interest to discuss briefly and to present relations governing equilibrium temperature distribution when certain common engineering models for thermal radiation properties are employed in analysis. Since surface roughness effects on properties are here limited to those on solar properties, Eq. (10) continues to apply, but analysis for $\mathcal{G}(\xi)$ is altered. The most general engineering model for surface properties in widespread use probably is the $\rho^D - \rho^S$ model which represents hemispherical reflectance (ρ) as the sum of a diffuse (ρ^D) and a specular (ρ^S) reflectance component. All directional dependence of surface properties is generally ignored. In addition to simplicity, use of the $\rho^D - \rho^S$ reflection model provides results for both limiting cases of diffusely reflecting and specularly reflecting surfaces. When this model is employed, dimensionless locally absorbed solar energy is given by[6]

$$\mathcal{G}(\xi) = (\alpha/\rho^D)\beta(\xi) \tag{13}$$

where $\beta(\xi)$ is dimensionless solar radiosity[6] and represents the ratio of diffusely distributed solar energy locally emergent from an element of surface area per unit time and per unit area to the value of S. $\beta(\xi)$ satisfies the following integral equation[6]:

$$\beta(\xi) = \rho^D\left[E(\xi) + \int_0^1 \beta(\eta)K_\gamma(\xi,\eta)d\eta\right] \tag{14}$$

where

$$E(\xi) = \sum_{j=0}^{M} (\rho^S)^j \sin\left[\frac{(2j+1)\gamma}{2}\right] U(\xi_j - \xi) \tag{15}$$

with

$$\xi_j = \sin(\gamma/2)/\sin[(2j+1)\gamma/2] \tag{16}$$

The symbol $U(\xi_j - \xi)$ denotes the unit step function which has the value 0 for negative arguments and 1 otherwise. The kernel K_γ in Eq. (14) is given by Eq. (2) with x, y, and $(1 - \epsilon)$ replaced with ξ, η, and ρ^S, respectively. As noted earlier, analysis employing this engineering model for surface properties does not require evaluation of solar intensity; the solar radiosity function is sufficient.

Results and comparisons are presented later which employ certain selected property values and reflection models in the formulation briefly summarized previously. One method employs material (wall) properties for solar energy; that is, $\alpha(= 1 - \rho) = \alpha_w$ and either a direction independent diffuse ($\rho^D = \rho$) or specular ($\rho^S = \rho$) reflection model. It is denoted as CW, which stands for constant-(direction-independent) property analysis using wall properties, and it neglects roughness effects on surface properties. The second method is denoted CA, for constant-property analysis using rough-surface, apparent directional absorptance for directly incident solar energy; that is, $\alpha(= 1 - \rho) = \alpha_a(\theta_S')$ and either a direction-independent diffuse or specular reflection model. CA analysis correctly evaluates directly incident solar energy locally absorbed by the rough surface and attempts to compensate for directional dependence of rough-surface properties in reflection phenomena by using a representative value for hemispherical reflectance with a specular or diffuse reflection model.

Rough Surface Radiation Properties

Our purpose here is simply to point out some important characteristics particularly pertinent to understanding results presented later. Rough-surface property results are presented and discussed in detail elsewhere.[1] In the cited study, all apparent properties for a one-dimensionally rough surface consisting of symmetric V-shaped roughness elements with identical included angle χ were reported. Asperity walls possessed direction-independent α_w, and reflection within roughness elements was described by a direction-independent reflectance model with a specular component ($\rho_w{}^S$) and a diffuse component ($\rho_w{}^D$). In addition to the material properties, apparent radiation properties depend on χ. Alternatively, the χ-dependence may be viewed as a dependence on surface roughness slope. The influence of the aforementioned parameters on rough-surface properties

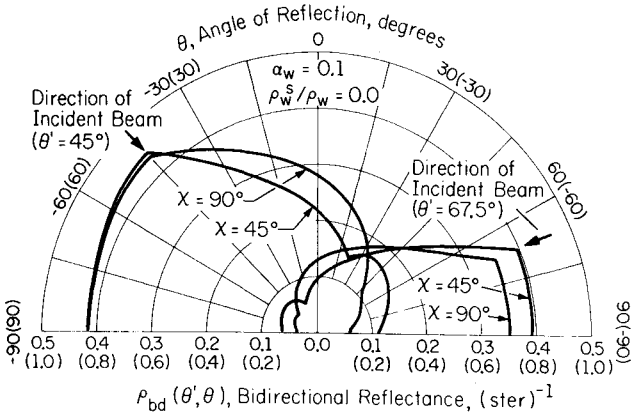

Fig. 2 Bidirectional reflectance for rough surface with diffusely reflecting roughness elements (scales in parentheses are for $\rho_{bd}(\theta',\theta)$ curves for $\theta' = 67.5°$).

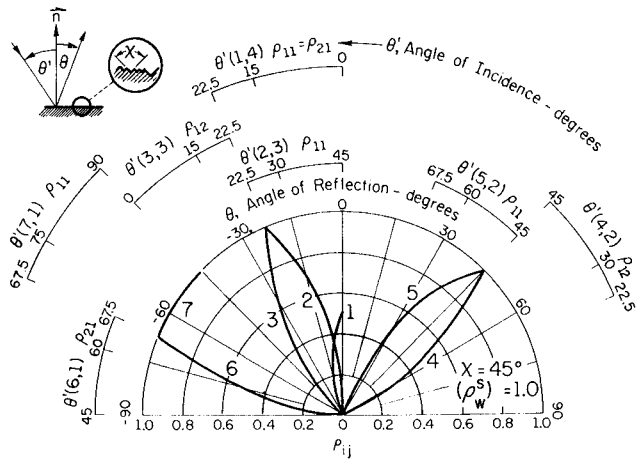

Fig. 3 Specular reflectance factors ($\chi = 45°$, $\rho_w{}^s = 1$).

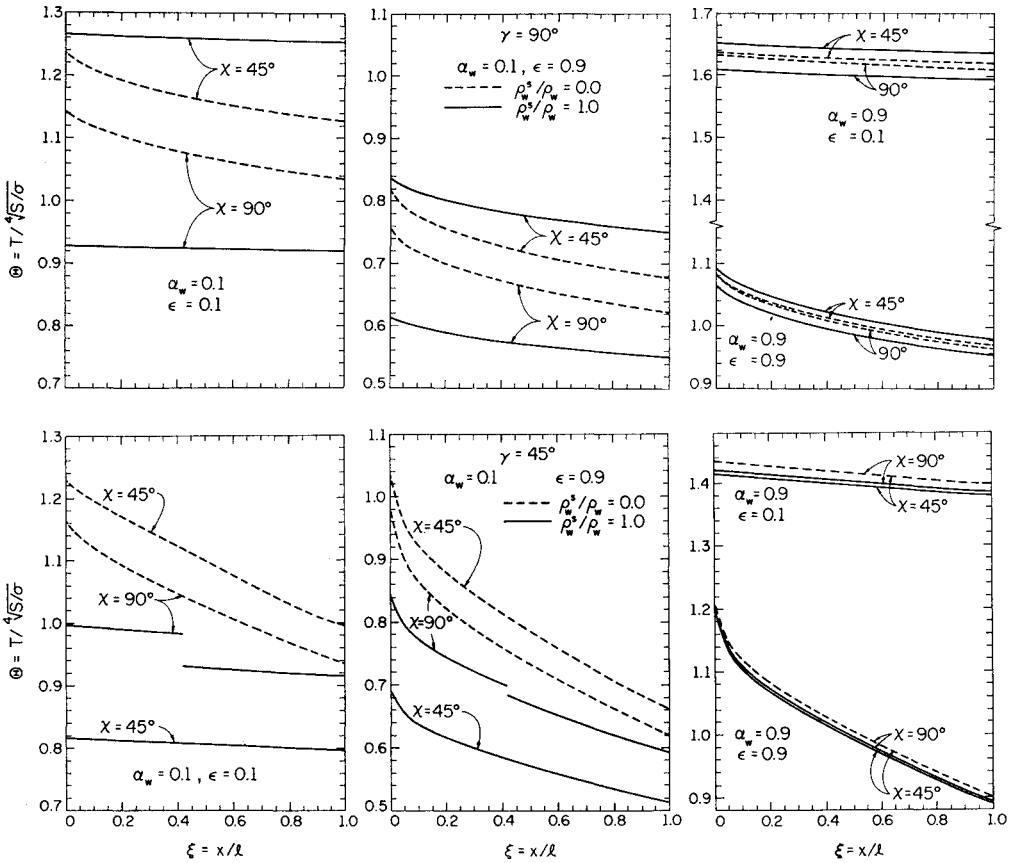

Fig. 4 Surface roughness effects on dimensionless equilibrium temperature distribution (top set: γ = 90°; bottom set: γ = 45°).

was expressed in terms of α_w, $\rho_w{}^s/\rho_w$, and χ. Some typical bidirectional reflectance results are illustrated in Figs. 2 and 3, while Table 1 presents results for apparent directional absorptance of the rough surface at selected directions of incidence for directly incident solar energy.

Although all rough-surface properties significantly differ from those commonly employed in radiant heat transfer analysis, their most striking feature is the concentration of reflected energy in directions at or near the direction of incident energy. In other words, the rough-surface bidirectional reflectance ρ_{bd} is dominated by a back-scattering characteristic. Figure 2 illustrates this characteristic. Although not included on the figure, a diffusely reflecting plane surface would be represented on this figure by a semicircle with radius ρ_w/π. The gross departure of the rough-surface ρ_{bd} from that for a diffusely reflecting plane surface is clearly evident.

Even more striking phenomena are suggested by the specular reflectance factors used to construct ρ_{bd} for specularly reflecting roughness elements[1] presented in Fig. 3. Consider the implication of the results of Fig. 3 for the system of surfaces considered here. Study reveals that for perpendicular plates (γ = 90°) directly incident solar energy undergoes an identical reflection path before exiting from the system for both the rough surface and a specularly reflecting smooth surface. According to Table 1, however, the energy absorbed at each interaction with the rough surface exceeds that for the smooth surface [$\alpha_a(\theta_S') > \alpha_w$] by a factor approaching 2 for low α_w (0.1) and by 10% for high α_w (0.9). Thus, all other factors being equal, local temperature of the rough surface will exceed that of the smooth surface, and the difference in temperature will increase with wall reflectance. On the other hand, when γ = 45° (θ_S' = 67.5°), all solar energy directly incident on the system is completely back-scattered and leaves the system without further reflection. For a specularly reflecting smooth surface, the directly incident solar energy undergoes interreflection between the surfaces before leaving the system. Since apparent directional absorptance of the rough surface for θ_S' = 67.5° is equal to α_w (see Table 1), local temperature of the rough surface will be less than that for the specularly reflecting smooth surface. An identical situation occurs for a rough surface with specularly reflecting roughness elements with the larger included angle (χ = 90°) when γ = 90°. For all three of these situations, analytical relations may be developed for $\mathcal{G}(\xi)$, and Eq. (12) need not be solved for solar intensity.

Method of Solution

Since only numerical results were available for the diffuse component of bidirectional reflectance, numerical techniques were generally employed to solve the integral equation governing dimensionless local solar intensity. The numerical methods employed are discussed elsewhere.[4] Intensity results were numerically integrated according to Eq. (11) to give $\mathcal{G}(\xi)$. For those situations cited in the previous section, analytical expressions were available and were used to evaluate $\mathcal{G}(\xi)$. Results for $\mathcal{G}(\xi)$ were employed in Eq. (10) to calculate $\Theta(\xi)$ using standard numerical techniques.[6] Numerical procedures were verified by calculating solar intensity, locally absorbed solar energy, and equilibrium temperature distributions for surfaces diffusely reflecting and specularly reflecting to solar energy and by comparing these results to those available in the literature.[6] The largest discrepancy in equilibrium temperature observed in all cases examined was 1%. As a result, it is estimated that rough-surface temperature results are accurate to within ~1%.

Results and Discussion

Typical dimensionless equilibrium temperature distributions are illustrated in Fig. 4. The upper and lower sets of figures are for included angles between the plates of 90° and 45°, respectively. Those to the left and in the center pertain to

materials of low solar absorptance ($\alpha_w = 0.1$) and those to the right to materials of high solar absorptance ($\alpha_w = 0.9$). In each figure, results are presented for χ's of 45° and 90° for both diffusely reflecting ($\rho_w{}^S/\rho_w = 0$) and specularly reflecting ($\rho_w{}^S/\rho_w = 1$) roughness elements. The general character of equilibrium temperature distribution in the adjoint plate system for diffusely and specularly reflecting surfaces has been fully discussed elsewhere[6]; attention is directed here to the influence of surface roughness on equilibrium temperature.

Consider the results for $\gamma = 90°$. First, the variation of temperature with χ and $\rho_w{}^S/\rho_w$ is identical for all combinations of values for α_w and ϵ. Local temperature is bounded by the results for surfaces with specularly reflecting roughness elements with those for the surface with greater roughness slope ($\chi = 45°$) yielding higher temperature. The intermediate temperatures attained by surfaces with diffusely reflecting asperities are also greater for the surface of larger roughness slope. This ordering of temperature is explained by the reflection phenomena which occur when the collimated solar energy interacts with the rough surface. Note that the reflection phenomena which occur when $\chi = 45°$ are very similar to those which occur when specular or diffuse analysis is employed.[6] Indeed, for specularly reflecting roughness elements, all directly incident solar energy is specularly reflected to the adjacent surface from which it is specularly reflected to the environment. For a diffusely reflecting surface, however, a significant portion of the incident energy is lost to the environment at each reflection. It follows that the local temperature acquired by the surface with specularly reflecting roughness elements will exceed that for the surface with diffusely reflecting elements.

The lower temperatures attained by the surface with diffusely reflecting elements of smaller roughness slope are inferred by the p_{bd} distributions of Fig. 2. For directly incident solar energy, a greater amount of energy is back-scattered for the surface with smaller roughness slope; hence, local solar irradiation and temperature should be less than for the surface of larger roughness slope. Now, as pointed out earlier, when the roughness elements are specularly reflecting and $\chi = 90°$, the directly incident solar energy is back-scattered and leaves the system without further reflection. Hence, solar irradiation is least for this situation and, therefore, temperatures are lowest. Of particular interest is the large variation in temperature attained by the rough surfaces of low α_w. The temperature for both low-ϵ and high-ϵ surfaces varies as much as 38% as the surface roughness parameters take on the limited values considered here. This percentage change in temperature translates into approximately 250°R for the temperature levels indicated in the figures. As should be expected, variation in local temperature with the roughness parameter values sharply diminishes as α_w increases, yielding temperatures for $\alpha_w = 0.9$, which differ by less than 3%. This is attributed to the diminishing contribution of reflected energy to local solar irradiation as solar absorptance increases.

Equilibrium temperature distributions presented in Fig. 4 for $\gamma = 45°$ have many of the same general trends as those already discussed for $\gamma = 90°$. Some significant differences however, do exist. First, as the roughness parameters are varied through their limited range, the low-α_w material attains temperatures as high as 50% greater than the lowest temperature. Second, in contrast to the results for $\gamma = 90°$, local temperature for surfaces with diffusely reflecting roughness elements exceeds that for surfaces with specularly reflecting elements. Again, the explanation of the relative local temperature values in terms of the roughness parameters lies in the reflection phenomena which occur in the system. Without going into detail, the situation for $\chi = 45°$ and $\rho_w{}^S/\rho_w = 1$ is identical to that discussed for $\gamma = 90°$ when $\chi = 90°$ and $\rho_w{}^S/\rho_w = 1$; that is, all directly incident solar energy is back-scattered out of the system. Hence,

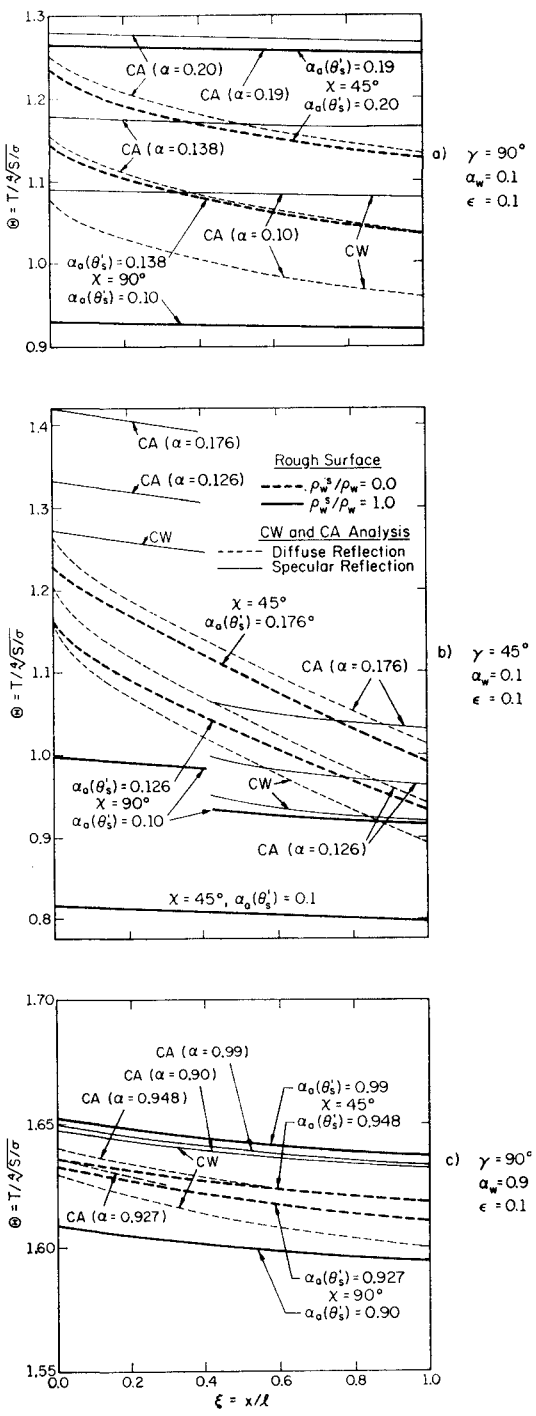

Fig. 5 Comparisons of results from approximate analysis with rough surface dimensionless equilibrium temperature distributions [see 5 b for key].

temperatures are lowest for this situation. For specularly reflecting roughness elements and the larger roughness included angle, complete back-scattering occurs only for a limited portion of the surfaces; the remaining energy emerges from the system after a finite number of reflections. The aforementioned back-scattering phenomena for surfaces with specularly reflecting roughness elements suggest that temperatures will be greater for surfaces with diffusely reflecting elements, and this is confirmed by the results of Fig. 4 for $\gamma = 45°$. The discontinuity in temperature evident in Fig. 4 is attributed to the lack of accounting for conductive transfer within the plates and the discontinuous nature of the local solar irradiation in the system. Finally, temperature results of Fig. 4 when $\gamma = 45°$ for high-α_w materials with

diffusely reflecting surface asperities and different roughness slope values are indistinguishable.

Of particular interest, is a comparison of rough-surface equilibrium temperature distribution to that evaluated using the radiation surface property models commonly employed in engineering analysis. Dimensionless equilibrium temperature distributions evaluated from rough-surface analysis, as well as those determined with the approximate methods previously denoted *CW* and *CA*, are illustrated in Fig. 5. Figures 5a and 5b present results for low-α_w, low-ϵ materials with γ's of 90° and 45°, respectively. The distributions in Fig. 5c pertain to a high-α_w, low-ϵ material with $\gamma = 90°$.

Consider first Fig. 5a. *CW* analysis with a specular reflection model yields equilibrium temperatures approximately equal to the arithmetic mean of those calculated for rough surfaces with specularly reflecting roughness elements and are, therefore, in error by ~15%. On the other hand, *CW* analysis with a diffuse reflection model predicts temperatures which are lower by 6–20% than those evaluated for rough surfaces with diffusely reflecting asperities. Significant improvement is observed when *CA* analysis is employed. When a diffuse reflection model is used, the equilibrium temperature results from *CA* analysis are less than 2% higher than those for the rough surface with diffusely reflecting roughness elements. This excellent agreement is somewhat surprising in view of the significantly different spatial distributions of reflected energy for a diffusely reflecting surface and a rough surface implied by Fig. 2. Although the lower temperatures for the rough surfaces testify to the greater back-scattering characteristics of the rough-surface bidirectional reflectance, apparently small energy differences are involved and, therefore, temperatures from the two analyses differ only slightly. *CA* analysis with a specular reflection model yields the rough surface temperature distribution for $\chi = 45°$ and $\rho_w{}^s/\rho_w = 1$. Neither *CA* nor *CW* analysis, however, yields an acceptable approximation to the rough surface temperature distribution when complete back-scattering of directly incident solar energy occurs as for $\chi = 90°$ and $\rho_w{}^s/\rho_w = 1$.

Temperature distributions presented in Fig. 5b for $\gamma = 45°$ confirm the general conclusions reached from the comparisons made for perpendicular plates. The discrepancy in temperature results between *CA* analysis, and that for the rough surface with diffusely reflecting asperities is approximately twice that observed for $\gamma = 90°$, but is less than a generally acceptable value of 4%. Again, when directly incident solar energy is dominated by back-scattering, such as for the rough surface with specularly reflecting roughness elements, the temperature error incurred by the use of *CA* analysis can be greater than 50%. *CW* analysis yields results in better agreement with the rough-surface temperature distribution in these situations principally because of the lower value for α_w.

Figure 5c presents a typical comparison of rough-surface equilibrium temperature distributions and results evaluated with *CW* and *CA* analysis. Both methods yield local temperatures which differ by less than 1½% from rough surface results. The superiority of *CA* analysis over *CW* analysis is clearly evident for rough surfaces with diffusely reflecting roughness elements.

Conclusion

The influence of surface roughness on the temperature acquired by radiatively adiabatic interacting surfaces in a collimated solar field has been studied. Characteristic lengths associated with the one-dimensional surface roughness profile were considered large relative to wavelengths of incident solar energy, but small relative to wavelengths for surface emitted energy. Surface roughness effects were relatively unimportant for materials of high solar absorptance (α_w), but the influence of surface roughness on equilibrium temperature T steadily increased as solar absorptance decreased. Local T for low-α_w materials increased by 50% as surface roughness slope and specularity varied over the range of values considered here. Rough-surface equilibrium temperature distributions were compared to those evaluated with two engineering methods of analysis that employed direction-independent specular or diffuse reflection models. Although a model which ignores roughness completely and uses material properties yields acceptable accuracy for high-α_w materials, it yields temperature errors as large as 50% for low-α_w materials. Significant improvement is generally obtained when engineering analysis employs rough surface apparent properties for directly incident solar energy. Temperature errors of less than 4% are incurred when the distribution of reflected energy from the rough surface is essentially distributed over hemispherical space even though significantly greater back-scattering occurs for the rough surface than for a diffusely reflecting surface. Neither method of analysis, however, yields acceptable temperature results for low-α_w materials when a large fraction of the directly incident solar energy is back-scattered to the environment without further reflection from system surfaces.

References

[1] Hering, R. G. and Smith, T. F., "Apparent Radiation Properties of a Rough Surface," *AIAA Progress in Astronautics and Aeronautics: Thermophysics: Applications to Thermal Design of Spacecraft*, Vol. 23, edited by J. T. Bevans, Academic, New York, 1970, pp. 337–361.

[2] Hering, R. G. and Smith, T. F., "Surface Roughness Effects on Equilibrium Temperature," *Journal of Spacecraft and Rockets*, Vol. 6, No. 8, Aug. 1969, pp. 955–957.

[3] Hering, R. G. and Smith, T. F., "Surface Roughness Effects on Radiant Heat Transfer," *Journal of Spacecraft and Rockets*, Vol. 6, No. 12, Dec. 1969, pp. 1465–1466.

[4] Hering, R. G. and Smith, T. F., "Surface Roughness Effects on Radiant Transfer between Surfaces," *International Journal of Heat and Mass Transfer*, Vol. 13, No. 4, April 1970, pp. 725–739.

[5] Hering, R. G., Smith, T. F., and Shaffer, J. T., "Surface Roughness Effects on Radiant Transfer between Surfaces," *Proceedings of Fourth International Heat Transfer Conference*, American Society of Mechanical Engineers, Vol. 3, 1970.

[6] Hering, R. G., "Radiative Heat Exchange and Equilibrium Surface Temperature in a Space Environment," *Journal of Spacecraft and Rockets*, Vol. 5, No. 1, Jan. 1968, pp. 47–54.